Fluid Dynamics & Materials Processing

Tech Science Press

DOI: 10.32604/fdmp.2023.043512

ARTICLE

Analysis of Calcined Red Mud Properties and Related Mortar Performances

Zhengfan Lyu[1,3], Yulin Li[2,3], Mengmeng Fan[1,3,*], Yan Huang[1] and Chenguang Li[2]

[1]Technical Center Office, Guangxi Jiaojian Engineering Inspection Consulting Co., Ltd., Nanning, 530001, China

[2]Technical Center Office, Guangxi Road Construction Engineering Group Co., Ltd., Nanning, 530001, China

[3]Nanning Road Construction Technology and Road Construction Materials Engineering Technology Research Centre, Guangxi Road Construction Engineering Group Co., Ltd., Nanning, 530001, China

[*]Corresponding Author: Mengmeng Fan. Email: fanmengmeng1712@163.com

Received: 04 July 2023 Accepted: 26 October 2023 Published: 07 June 2024

ABSTRACT

Red mud (RM) is a low-activity industrial solid waste, and its utilization as a resource is currently a hot topic. In this study, the micro characteristics of red mud at different calcination temperatures were analyzed using X-ray diffraction and scanning electron microscopy. The performance of calcined red mud was determined through mortar strength tests. Results indicate that high-temperature calcination can change the mineral composition and microstructure of red mud, and increase the surface roughness and specific surface area. At the optimal temperature of 700°C, the addition of calcined red mud still leads to a decrease in mortar strength, but its activity index and flexural coefficient increase by 16.2% and 11.9% with respect to uncalcined red mud, reaching values of 0.826 and 0.974, respectively. Compared with the control group, the synergistic activation of calcined red mud with slag can increase the compressive and flexural strength of the mortar by 12.9% and 1.5%, reaching 8.7 and 62.4 MPa, respectively. Correspondingly, the activity index and flexural coefficient of the calcined RM and GGBS (Ground Granulated Blast furnace Slag) mixtures also increase to 1.015 and 1.130, respectively.

KEYWORDS

Red mud; slag; thermal activation; synergistic activation; mortar test; microscopic properties

1 Introduction

Red mud (RM) is a solid waste produced in the alumina process, which is figuratively called RM because of its high iron content and reddish-brown colour [1]. Due to the significant amount of caustic soda added in the process of alumina production for leaching aluminum from the ore, the discharged RM exhibits a high alkalinity [2]. Its pH value can usually be as high as 11.0~12.0 [3]. According to the International Aluminum Institute, the total global alumina production in 2022 reached 139 million tonnes, and the production of 1 tonnes of alumina generally results in the generation of about 1~1.5 tonnes of RM [4]. This means that in 2022 alone, the world has generated 139~208 million tons of RM. The massive storage of RM not only occupies a large amount of land, but also poses the risk of soil alkalization [5,6] and water pollution [7–9] in the surrounding areas in the event of leakage. RM is an aluminum-silica-rich material [10,11] and is a high-quality raw material for the preparation of construction materials. However, Bayer RM is inherently less active, and untreated RM is usually not

available as an effective component of construction materials. Therefore, it is necessary to carry out activation studies for RM treatment.

RM activation treatment methods having been used include mechanical activation, high-temperature thermal activation, alkali chemical activation and synergistic activation. In this regard, scholars have carried out corresponding studies. Li et al. [12] found that utilizing mechanical activation can improve the early activity of RM. Singh et al. [13] investigated the effect of mechanical activation on the strength of RM-fly ash geopolymer slurry. They found out that mechanical activation facilitated the reaction between the hematite phase and silica in RM, resulting in higher strength of geopolymer slurry incorporating mechanically ground RM. Dong et al. [14] explored the effects of calcination temperature and time on the activation effect of RM. The results showed that a continuous calcination time of 60 min at 500°C yielded the most favorable activation effect on the RM. According to Hou et al. [15], the optimal thermal activation condition for the RM was calcination at 600°C for 3 h. Correspondingly, the 28 d compressive strength of the cement mortar blended with the calcined RM increased by 15.3% compared to the non-calcined state, reaching 27.0 MPa. Luo et al. [16] studied the effect of the amount of calcined RM at different temperatures on the compressive strength and microstructure of cement mortar. The results reported that the mineral composition of RM changes after being calcined at 900°C, and the 28 d compressive strength of cement mortar blended with 15% calcined RM was superior to that of pure cement mortar. Due to the strong alkaline properties of RM, the effect of using alkaline excitation method to activate RM is usually not significant [17], and it will further increase the alkalinity of the RM. Therefore, some scholars have conducted activation studies on RM based on the synergistic utilization theory. Kancir et al. [18] found high synergy between red mud, calcined clay and limestone, which can be used as supplementary cementitious materials to reduce the use of cement. Hao et al. [19] found a good gelling synergy between steel slag, desulfurization gypsum and RM. The alkali in RM and sulfate in desulfurization gypsum can effectively activate the chemical reactivity of steel slag, and promote the generate of C-S-H gel and ettringite. Zhang et al. [20] prepared a multi-solid waste cementitious material containing RM, converter steel slag and blast furnace slag. The study revealed that the optimal synergistic effect among the three solid waste materials occurred when the converter steel slag content is 30 wt%. By adding this material to P-I 42.5 cement, the strength grade can reach the level of P-C 52.5 cement. The above studies have shown that the treatment of RM through high-temperature thermal activation and synergistic activation can effectively improve its activity. Nonetheless, there are certain differences in the chemical mineral composition of RM in different regions, so the activation conditions of RM may also be different. Moreover, the current studies mainly focused on low-iron and high-calcium RM and high-iron and low-calcium RM [13–20].

Based on the previous research, the high-iron and high-calcium Bayer RM is used as the research object in the present study. Firstly, the effects of different calcination temperatures on the microscopic properties of RM were explored. Then, the performance of thermally activated RM was studied through mechanical performance tests of mortar. This study tends to provide a certain scientific basis for the comprehensive utilization of Bayer RM.

2 Experiments

2.1 Raw Materials

RM is Bayer red mud supplied from Aluminum Corporation of China's Limited Guangxi Branch. Ground Granulated Blastfurnace Slag (GGBS) was produced by Guangxi Yuan Sheng Slag Comprehensive Utilization Co., Ltd., China. The cement (PC) is Chinese Portland cement (P·O 42.5), produced by Guangxi Yufeng Cement Company, China. The test employed ISO standard sand, manufactured by Xiamen Aisiou, China. The water used for the test was ordinary tap water. The chemical

compositions of cement, GGBS and RM, were determined using an X-ray fluorescence spectroscopy analyzer (XRF), as presented in Table 1. Other performance indicators of cement are shown in Table 2.

Table 1: Main chemical composition of raw materials

Chemical composition	Na_2O	Fe_2O_3	Al_2O_3	SiO_2	CaO	TiO_2	SO_3	MgO	K_2O	MnO
RM (%)	10.90	28.80	18.50	15.75	15.72	6.66	0.71	0.25	0.24	0.11
GGBS (%)	0.43	0.40	14.95	31.90	37.80	0.66	2.08	7.91	0.30	0.35
PC (%)	0.28	3.20	5.55	21.47	62.58	/	1.85	3.72	0.63	/

Table 2: Cement performance indicators

Fineness $m^2 \cdot kg^{-1}$	Normal consistency %	Initial setting time min	Final setting time min	28 d compressive strength MPa	28 d flexural strength MPa
364	26.8	165	284	61.5	7.7

2.2 Activation of Red Mud

The thermal activation process of RM is shown in Fig. 1.

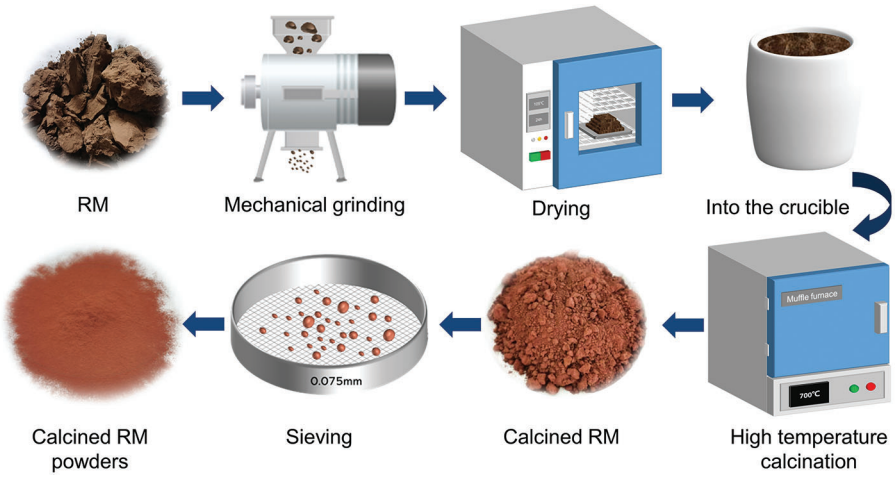

Figure 1: Thermal activation process of RM

Firstly, the RM was dried in a drying oven (105°C ± 5°C) for 24 h to remove the moisture from the RM. The dried RM was then ground using a powder mill. Subsequent high-temperature thermal activation of the RM in a muffle furnace. In this study, RM was calcined at different temperatures ranging from 600°C to 1000°C. According to references [14–16], we set the gradient of calcination temperature to 100°C. When the temperature reached the set value, calcination began and lasted for 3 h. Finally, the completed thermally activated RM was passed through 0.075 mm standard sieve and kept sealed for use. Synergistic activation: GGBS is evenly mixed with RM and calcined RM at optimal temperature in the ratio of 1:1, respectively, to make the composite admixture.

2.3 Mix Proportion

According to the above test scheme, a total of 10 sets of mortars with varying proportions were designed for this experiment. Within these groups, one group comprised of pure cement mortar was designated as the control group. The detailed proportions are shown in Table 3 below. In Table 3, CM refers to pure cement mortar, CRM-600 refers to the cement mortar containing 600°C calcined RM (and so on), CGM refers to the cement mortar containing GGBS, CRGM refers to the cement mortar containing RM and GGBS, and CHRGM refers to the cement mortar containing calcined RM and GGBS.

Table 3: Proportion of raw materials

Test number	Calcination temperature of RM °C	Cement %	RM %	GGBS %
CM	/	100	/	/
CRM	/	70	30	/
CRM-600	600			
CRM-700	700			
CRM-800	800			
CRM-900	900			
CRM-1000	1000			
CGM	/	70	/	30
CRGM	/		15	15
CHRGM	700		15	15

2.4 Sample Preparation and Curing

The preparation and Curing of the samples in this study were referred to Chinese Standard GB/T 17671-2021 "Test method of cement mortar strength (ISO method)". Firstly, 450 g of cementitious material (cement to admixture ratio 7:3), 1350 g of ISO standard sand, and 225 g of water were weighed. Next, mortar samples with dimensions of 40 mm × 40 mm × 160 mm, with 3 samples per group, were prepared in a laboratory at an ambient temperature of 20°C ± 2°C and relative humidity ≥50%. Subsequently, the samples, along with the test molds, were placed in a curing chamber at the temperature of 20°C ± 1°C and the relative humidity of ≥90% for curing. After 24 h, the mold was removed and each group of samples was transferred to a separate water tank (at a temperature of 20°C ± 1°C) for curing. Finally, the samples were removed after 28 days of curing for mechanical property testing. The prepared samples are shown in Fig. 2.

Figure 2: Mortar sample

2.5 Test Method

2.5.1 Mechanical Properties

Mechanical properties were tested on a ETM305-2 microcomputer-controlled electronic compressive and flexural testing machine (produced by Shenzhen Wance Testing Equipment Co., Ltd., Shenzhen, China). According to Chinese Standard GB/T 17671-2021 "Test method of cement mortar strength (ISO method)", the loading speed for compressive strength testing and flexural strength testing were set at 2400 ± 200 N/s and 50 ± 10 N/s, respectively. The arithmetic mean of the measured values of the three samples was used as the test result. Fig. 3 shows a picture of the mechanical performance testing.

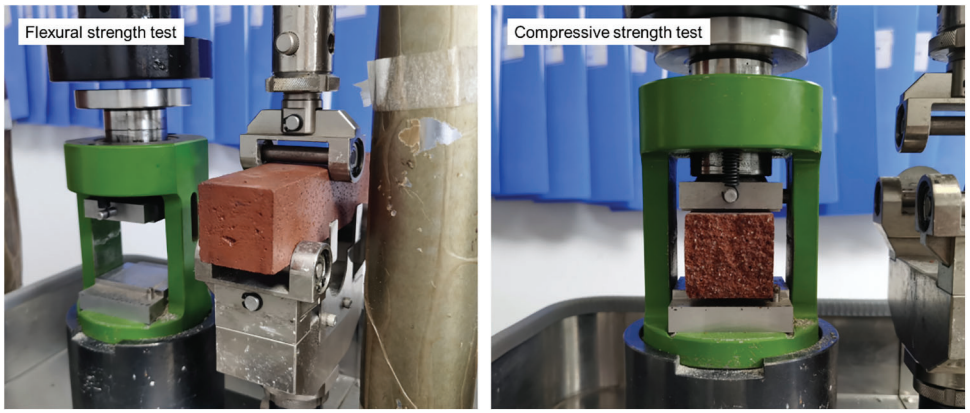

Figure 3: Mechanical performance testing

2.5.2 Activity Index and Flexural Coefficient

Referring to Chinese Standard GB/T1596-2017 "Fly ash used for cement and concrete", the activity index H_{28} and flexural coefficient F_{28} of RM can be expressed as the Eqs. (1) and (2). The method in Section 2.4 was employed to prepare mortar specimens and test the 28 d unconfined compressive strength and 28 d flexural strength of each group of mortar specimens respectively. The activity index and flexural coefficient of the RM were obtained by substituting the obtained test results into the following equations:

$$H_{28}=\frac{R_{u1}}{R_{u2}} \tag{1}$$

$$F_{28}=\frac{R_{f1}}{R_{f2}} \tag{2}$$

where R_{u1} and R_{f1} refer to the 28 d unconfined compressive strength and 28 d flexural strength of cement mortar mixed with RM or GGBS, respectively, while R_{u2} and R_{f2} refer to the 28 d unconfined compressive strength and 28 d flexural strength of cement mortar, respectively.

2.5.3 Microscopic Analysis

In this study, an X-ray diffractometer (XRD) and a scanning electron microscope (SEM) were used to analyze the microscopic properties of RM. The mineral composition data of RM at different calcination temperatures was obtained by Rigaku D/MAX 2500V XRD (produced by Rigaku-Corporation, Japan). The XRD scanning range was set from 5° to 75°, employing an operating voltage of 40 kV and a current of 150 mA. The microscopic morphology of RM particles at different calcination temperatures was observed using an S-3400N SEM (produced by Hitachi Limited, Japan). The operating voltage of SEM was set at 15 kV and the observation magnification was 2000 times.

3 Results and Discussion

3.1 Microscopic Properties of Calcined RM

3.1.1 XRD Analysis

Fig. 4 illustrates the XRD spectra of the RM following heat treatment at various calcination temperatures.

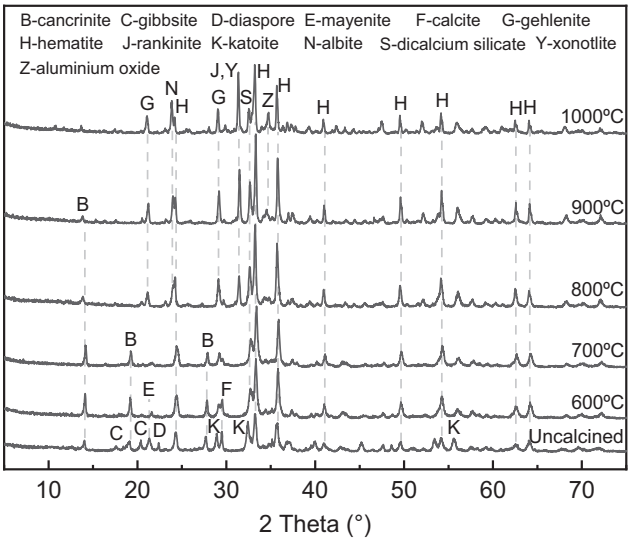

Figure 4: XRD spectrum of calcined RM

As can be seen from Fig. 4, the main mineral composition in the uncalcined RM includes cancrinite, gibbsite, diaspore, mayenite, calcite, katoite and hematite. After the thermal activation treatment at different temperatures, the mineral composition in RM, except for hematite, exhibit varying degrees of transformation. At 600°C, the XRD characteristic peaks of calcite and mayenite exhibit a decrease. This is due to the lower crystallinity of calcite in RM, which can decompose at this temperature [21]. At the same time, mayenite also undergoes phase transformation at this temperature [22]. In addition, the characteristic peaks of katoite, gibbsite and diaspore disappear at this temperature, where katoite may have reacted with the alkaline component of RM to form cancrinite, which elevates the characteristic peaks of cancrinite at $2\theta = 14.1°$ and 19.2°. Gibbsite and diaspore decompose to form alumina (Al_2O_3), but the characteristic peaks of alumina was not observed on the XRD curve at this temperature. This result suggests that the generated alumina may be amorphous, which may contribute to the RM activity. At 700°C, due to the increase in temperature, the characteristic peaks of calcite and mayenite almost completely disappear, where mayenite transforms into a weaker bulge peak in the range $2\theta = 21°\sim22°$. It indicates that amorphous active substances containing calcium, aluminum, and silicon elements generated in RM. At 800°C or higher, three new mineral phases are produced in the RM, containing gehlenite, albite, and rankinite. This indicates the initiation of the sintering in the RM, resulting in a decrease in the content of amorphous mineral composition, which is unfavorable for stimulating RM activity. With a further increase in the calcination temperature, there is an observed increase in the characteristic peaks of gehlenite, albite and rankinite, indicating an intensification of sintering phenomenon in RM. Notably, XRD peaks of alumina crystals were produced in the RM when calcination temperatures reach 900°C and 1000°C, probably formed by the action of amorphous alumina at high temperatures.

3.1.2 SEM Analysis

The microscopic morphology of the RM particles after calcination at different temperatures is shown in Fig. 5.

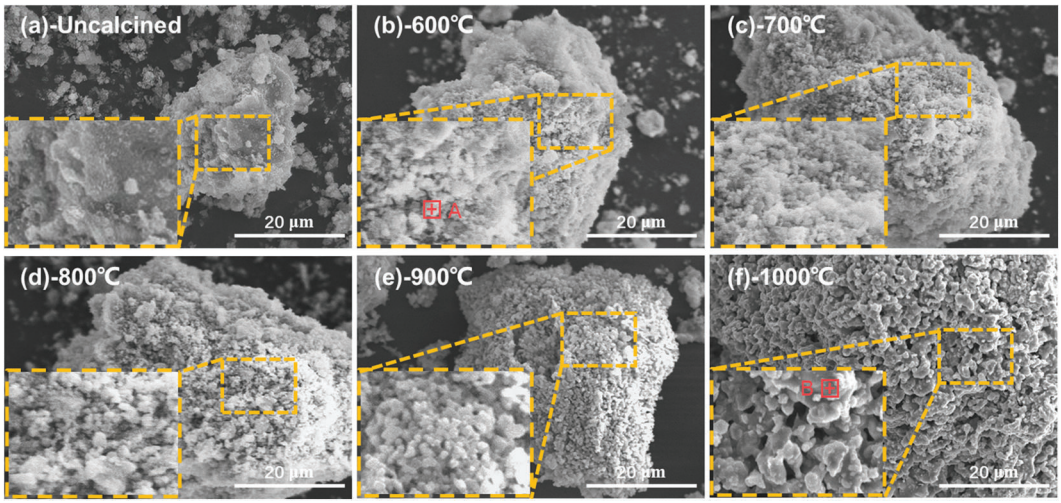

Figure 5: SEM image of calcined RM

As can be seen in Fig. 5, the surface of the uncalcined RM particles appears relatively smooth. However, the surface of RM becomes rough after high-temperature calcination at 600°C, for many tiny particles are generated on the surface of the RM, forming a pore structure resembling a honeycomb. Element analysis was performed on these articles using Energy Dispersive X-ray Spectrometer (EDS) (shown in Fig. 6a), revealing that the main elements of these particles include calcium, aluminum, and silicon. Therefore, it can be inferred that these particles are amorphous active minerals generated by high-temperature action. In addition, the appearance of these particles is also the reason for the changes in the surface morphology of RM. When the calcination temperature of the RM reaches 700°C and 800°C, the content of tiny particles on the surface of the RM increases significantly, the surface pore structure becomes more abundant, and the surface roughness and specific surface area increase correspondingly. In general, the larger the specific surface area of the material, the higher the surface activity. For RM, therefore a larger specific surface area can facilitate the excitation of its mineral activity, containing elemental aluminium and silica. As the calcination temperature continues to rise, the surface morphology of the RM undergoes further changes. Specifically, at 900°C, the content of small particles on the surface of RM significantly decreases, while a large number of particles in larger size appear, which was even more pronounced at 1000°C. This may be attributed to the significant presence of free alkalis and chemically bound alkalis in the RM [23,24]. When the calcination temperature is too high, the tiny particles on the surface of RM tend to sinter under the influence of alkalis, causing them to interconnect with each other and block the pore channels between the particles [25]. The result is a sharp decrease in the specific surface area of RM, which is not conducive to the activation of active substances in RM. From the EDS test results shown in Fig. 6b, it can also be observed that the proportion of sodium element significantly increases at the sintering site on the surface of calcined RM, which confirms that the sintering of RM is related to alkaline composition.

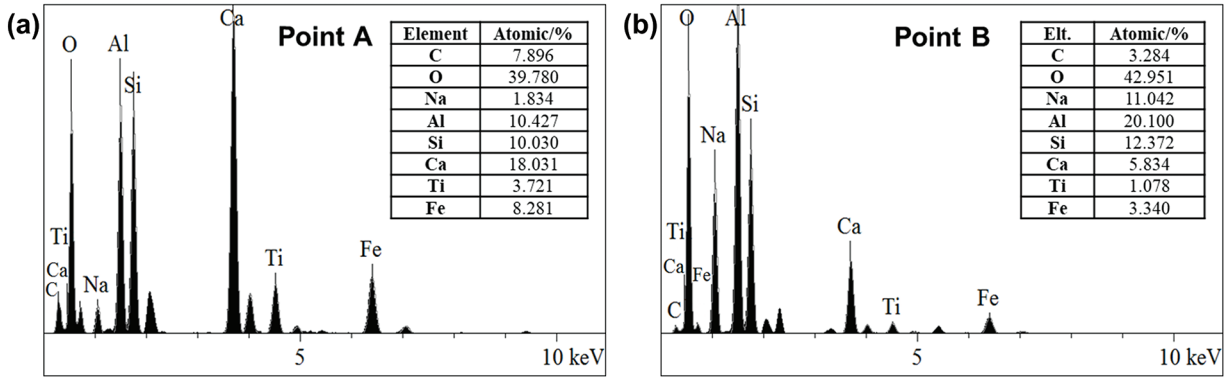

Figure 6: Elemental analysis results of calcined RM surface particles

3.2 Mechanical Strength of Mortars with Thermally Activated RM

Figs. 7 and 8 show the mechanical properties of the cement-RM mortar at different calcination temperatures as well as the activity index and flexural coefficient of the calcined RM, respectively.

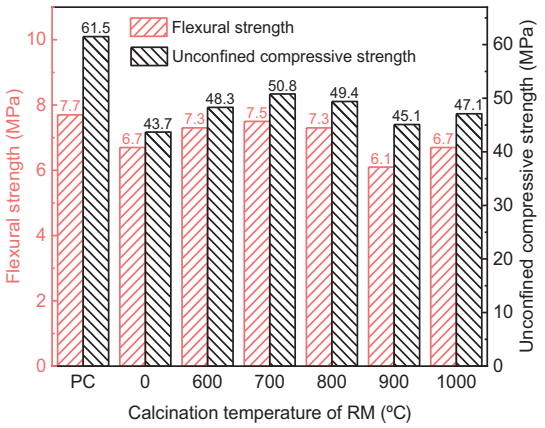

Figure 7: Mechanical properties of cement-RM mortars at different calcination temperatures

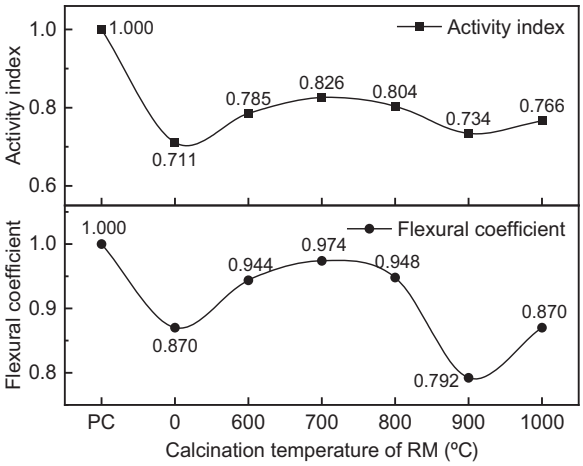

Figure 8: Activity index and flexural coefficient of calcined RM

As can be seen from Figs. 7 and 8, when the calcination temperature of RM increases, the mechanical properties of CRM and activity index of RM exhibit a pattern of initial increase, followed by decrease, and then increase again. At the calcination temperature of 700°C, both the mechanical properties of CRM and the activity index of RM reach their optimal values under thermal activation conditions. At this temperature, the 28 d unconfined compressive strength of CRM is 50.8 MPa, and the activity index of RM has increased by 16.2%, reaching 0.826. This performance enhancement is mainly due to the formation of active minerals containing calcium, aluminum and silicon in calcined RM, which are able to undergo a secondary hydration reaction with calcium hydroxide produced by cement hydration and generate C-S-H [26,27]. However, the beneficial effect of thermal activation on the RM starts to diminish when the calcination temperature exceeds 700°C. For instance, at a temperature of 900°C, the 28 d unconfined compressive strength of CRM is merely 45.1 MPa, and the activity index of RM also drops sharply to 0.734. The reason is that, seen from the results of microscopic analysis, on the one hand, the RM generates less active phases such as gehlenite and albite at this high temperature [28], leading to a decrease in the amount of active minerals; on the other hand, although some alumina crystals potentially beneficial for enhancing activity are generated in RM, the sintering phenomenon of RM inhibits the participation of alumina in the reaction. It is noteworthy that the mechanical properties of CRM and the RM activity index exhibit partial recovery when the calcination temperature increases to 1000°C. According to the SEM analysis, this may be related to the larger particle gap on the surface of the RM calcined at 1000°C, which is more conducive to the full reaction of the alumina. In addition, at 1000°C, albite is produced in RM. Despite the low activity of albite, under the alkaline environment provided by cement and RM, albite undergoes ion exchange reaction, gradually dissolves, and generates geopolymer gel [29]. This reaction is easier for RM calcined at 1000°C with a larger surface particle gaps.

In terms of flexural properties, the 28 d flexural coefficient of RM calcined at 600°C~800°C ranges from 0.944 to 0.974, with the CRM maximum flexural strength of 7.5 MPa. This result indicates that replacing cement with RM calcined at the appropriate temperature has a minimal impact on the flexural strength of cement mortar. The reason for this is that, on one hand, the high-temperature calcination increases the chemical reactivity of the RM; on the other hand, the calcined RM with a rough surface also can be better adhesive with the hydration products of cement. This also alleviates the problem of flexural strength degradation to some extent.

In summary, thermal treatment is an effective way to enhance the activity of Bayer RM. For the RM in this study, the optimal temperature of thermal treatment is around 700°C.

3.3 Mechanical Strength of Mortars Containing Calcined RM and GGBS

In order to investigate the effect of thermal activation on the synergistic effect of RM-GGBS, a composite admixture of 700°C calcined RM and GGBS was employed to prepare a cement mortar. The test results are shown in Figs. 9 and 10.

As can be seen from Figs. 9 and 10, compared with the CM group, the 28 d unconfined compressive strength of the mortar in CGM group decreases by 1.2 MPa, while the flexural strength increases by 0.4 MPa. Correspondingly, the 28 d activity index and the flexural coefficient of GGBS are 0.981 and 1.052, respectively. This demonstrates that replacing a portion of the cement with GGBS has a minor impact on the mortar's compressive strength and improves its flexural strength. As for the CRGM group, the 28 d unconfined compressive strength reduces to 58.0 MPa, compared with the CGM group. The 28 d activity index of the RM-GGBS composite admixture correspondingly reduces to 0.944, but is still significantly higher than that of the RM-doped CRM group. Different from the decrease in compressive strength, the flexural strength of the CRGM group was 0.4 MPa higher than that of the CGM group. The flexural coefficient of RM-GGBS composite admixture also increases from 1.052 to 1.104 accordingly. The improvement is more significant compared with the CM group. This result reveals that the mixture of

RM and GGBS can effectively enhance the flexural strength of mortar, and also indicates RM is an active ingredient in the composite admixture. However, the results of the compressive strength tests indicate that using GGBS alone for synergistic activation of RM cannot achieve optimal activation of RM. For the CHRGM group, the 28 d flexural strength and 28 d unconfined compressive strength are 8.7 and 62.4 MPa, respectively, higher than the rest of the groups. The flexural coefficient and activity index of the composite admixture composed of calcined RM and GGBS also correspondingly increase, reaching 1.130 and 1.015, respectively. This also demonstrates that thermal activation enhances the synergistic effect between RM and GGBS. The reason may be that the active minerals in the calcined RM can consume cement to generate calcium hydroxide [26,27], promoting continuous hydration of cement and generating new calcium hydroxide. These calcium hydroxides in turn promote the reaction of GGBS [30–33].

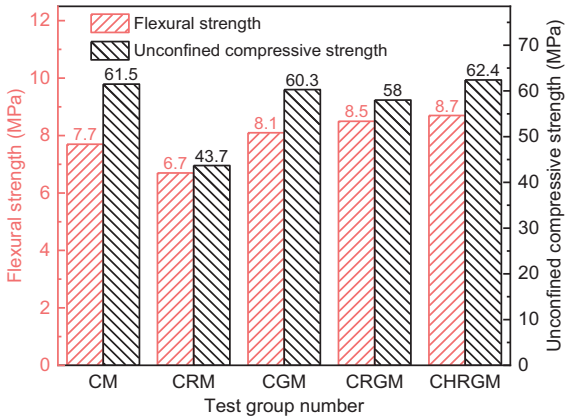

Figure 9: Mechanical properties of mortar under thermal activation-coactivation effect

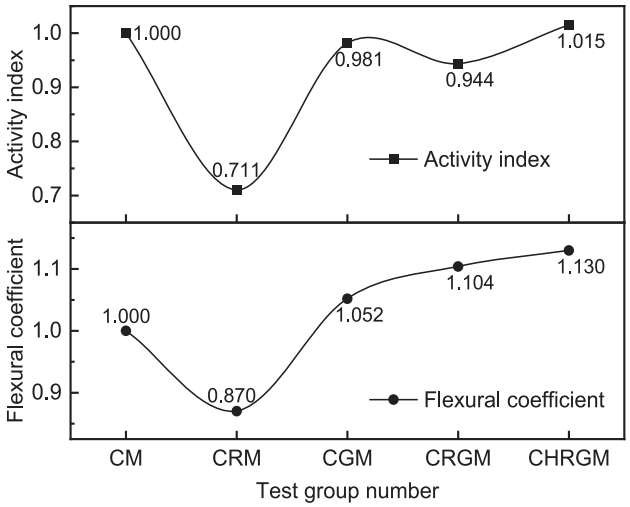

Figure 10: Comparison of activity index and flexural coefficient

4 Conclusion

This study focuses on Bayer RM in Pingguo City, Guangxi. An experimental program was conducted to study the microscopic properties of calcined RM, as well as the activity index and properties of thermal activated RM and synergistic activated RM. The following conclusions can be drawn:

1. The microscopic analysis results indicate that high-temperature calcination can change the mineral composition of RM, promote the generation of amorphous active minerals containing calcium, aluminum, and silicon elements, thereby changing the surface morphology of RM and increasing its surface roughness and specific surface area. However, excessive calcination temperature can lead to sintering phenomenon in RM, which blocks the pores among RM surface particles, which is not conducive to the activation of RM.

2. The optimal activation temperature of RM in Pingguo, Guangxi is around 700°C. At this optimal temperature, the compressive strength and flexural strength of cement mortar containing calcined RM have increased by 16.2% and 11.9%, respectively. Thermal activation, therefore, is an effective way to increase RM activity.

3. The flexural and compressive performance of cement mortar containing calcined RM and GGBS are not only higher than that of cement mortar containing uncalcined RM and GGBS, but also higher than that of pure cement mortar. This demonstrates that thermal activation can enhance the synergistic effect between RM and GGBS.

Acknowledgement: The authors greatly appreciate Liu Si graduated from Guangdong University of Foreign Studies for her English proofreading work.

Funding Statement: This study was supported by the "Key Science and Technology Project of Guangxi Department of Communications—Technology Development and Application of Cement Red Clay Stabilized Sea Sand Semi-Rigid Subgrade" (Grant: Gui Jiaotong 2020-No. 150) and "Key Science and Technology Project of Guangxi Department of Transportation—Key Technologies and Application Demonstrations for the Multi-Solid Waste Co-Processing of Bayer Red Mud in Large-Scale Road Construction" (Grant: Gui Jiaotong 2021-No. 148).

Author Contributions: Study conception and design: Zhengfan Lyu, Mengmeng Fan; data collection: Yulin Li; analysis and interpretation of results: Zhengfan Lyu, Yan Huang; draft manuscript preparation: Zhengfan Lyu, Chenguang Li. All authors reviewed the results and approved the final version of the manuscript.

Availability of Data and Materials: The authors confirm that the data supporting the findings of this study are available within the article.

Conflicts of Interest: The authors declare that they have no conflicts of interest to report regarding the present study.

References

1. Sadangi, J., Das, S., Tripathy, A., Biswal, S. (2018). Investigation into recovery of iron values from red mud dumps. *Separation Science and Technology, 53(14),* 2186–2191. https://doi.org/10.1080/01496395.2018.1446984
2. Suchita, R., Nimje, M., Chaddha, M., Modak, S., Rao, K. et al. (2019). Recovery of iron from bauxite residue using advanced separation techniques. *Minerals Engineering, 134,* 222–231. https://doi.org/10.1016/j.mineng.2019.02.018
3. Xue, S., Zhu, F., Kong, X., Wu, C., Huang, L. et al. (2016). A review of the characterization and revegetation of bauxite residues (red mud). *Environmental Science and Pollution Research, 23,* 1120–1132. https://doi.org/10.1007/s11356-015-4558-8

4. Brunori, C., Cremisini, C., Massanisso, P., Pinto, V., Torricelli, L. (2005). Reuse of a treated red mud bauxite waste: Studies on environmental compatibility. *Journal of Hazardous Materials, 117(1),* 55–63. https://doi.org/10.1016/j.jhazmat.2004.09.010
5. Rékási, M., Feigl, V., Uzinger, N., Gruiz, K., Makó, A. et al. (2013). Effects of leaching from alkaline red mud on soil biota: Modelling the conditions after the hungarian red mud disaster. *Chemistry and Ecology, 29(8),* 709–723. https://doi.org/10.1080/02757540.2013.817568
6. Winkler, D., Bidló, A., Bolodár-Varga, B., Erdő, Á., Horváth, A. (2018). Long-term ecological effects of the red mud disaster in hungary: Regeneration of red mud flooded areas in a contaminated industrial region. *The Science of the Total Environment, 644,* 1292–1303. https://doi.org/10.1016/j.scitotenv.2018.07.059
7. Agrawal, V., Paulose, R., Arya, R. (2022). Green conversion of hazardous red mud into diagnostic X-ray shielding tiles. *Journal of Hazardous Materials, 424,* 127507. https://doi.org/10.1016/j.jhazmat.2021.127507
8. Schöll, K., Szövényi, G. (2011). Planktonic Rotifer assemblages of the Danube river at Budapest after the red sludge pollution in Hungary. *Bulletin of Environmental Contamination and Toxicology, 87,* 124–128. https://doi.org/10.1007/s00128-011-0331-y
9. Olszewska, J. P., Heal, K. V., Edwards, R., McDonald, C., Foster, T. et al. (2019). Assessing the legacy of red mud pollution in a shallow freshwater lake: Long-term chemical recovery in the water column. *Inland Waters, 9(4),* 453–463. https://doi.org/10.1080/20442041.2018.1561083
10. Shrey, A., Nikhil, D. (2021). Investigation of mechanical and thermal activation on metal extraction from red mud. *Sustainable Materials and Technologies, 27,* e00246. https://doi.org/10.1016/j.susmat.2021.e00246
11. Shrey, A., Nikhil, D. (2022). Process flowsheet for extraction of Fe, Al, Ti, Sc, and Ga values from red mud. *Minerals Engineering, 184,* 107601. https://doi.org/10.1016/j.mineng.2022.107601
12. Li, Y., Min, X., Ke, Y., Liu, D., Tang, C. (2019). Preparation of red mud-based geopolymer materials from MSWI fly ash and red mud by mechanical activation. *Waste Management, 83,* 202–208. https://doi.org/10.1016/j.wasman.2018.11.019
13. Singh, S., Aswath, M. U., Ranganath, R. V. (2018). Effect of mechanical activation of red mud on the strength of geopolymer binder. *Construction and Building Materials, 177,* 91–101. https://doi.org/10.1016/j.conbuildmat.2018.05.096
14. Dong, P., Yin, D., Han, Y. (2022). Improvement of red mud activity and its effect on the properties of cement clinker. *New Building Materials, 49(1),* 28–30 (In Chinese).
15. Hou, S., Gao, S., Zhang, L., Li, N., Zhu, Y. (2020). Effects of thermal and mechanical activation on properties of bayer red mud. *Bulletin of the Chinese Ceramic Society, 39(5),* 1573–1577 (In Chinese).
16. Luo, S., Liu, M., Yang, L., Chang, J., Yang, W. (2019). Utilization of waste from alumina industry to produce sustainable cement-based materials. *Construction and Building Materials, 229(30),* 116795.
17. Ye, N., Yang, J., Ke, X., Zhu, J., Li, Y. (2014). Synthesis and characterization of geopolymer from bayer red mud with thermal pretreatment. *Journal of the American Ceramic Society, 97(5),* 1652–1660. https://doi.org/10.1111/jace.2014.97.issue-5
18. Kancir, V., Serdar, M. (2022). Contribution to understanding of synergy between red mud and common supplementary cementitious materials. *Materials, 15(5),* 1968. https://doi.org/10.3390/ma15051968
19. Hao, X., Liu, X., Zhang, Z., Zhang, W., Lu, Y. (2022). In-depth insight into the cementitious synergistic effect of steel slag and red mud on the properties of composite cementitious materials. *Journal of Building Engineering, 52,* 104449. https://doi.org/10.1016/j.jobe.2022.104449
20. Zhang, W., Hao, X., Wei, C., Zeng, Q., Ma, S. (2022). Synergistic enhancement of converter steelmaking slag, blast furnace slag, Bayer red mud in cementitious materials: Strength, phase composition, and microstructure. *Journal of Building Engineering, 60,* 105177. https://doi.org/10.1016/j.jobe.2022.105177
21. Dong, L., Ni, W., Zheng, Y., Li, X., Yv, J. et al. (2008). Research on preparation of low-clinker cementitious material via heat treatment of red mud and fly ash. *Environmental Engineering, 3,* 92–95+6 (In Chinese).
22. Tolkacheva, A., Shkerin, S., Korzun, I., Plaksin, S., Plaksin, S. et al. (2012). Phase transition in mayenite $Ca_{12}Al_{14}O_{33}$. *Russian Journal of Inorganic Chemistry, 57(7),* 1014–1018. https://doi.org/10.1134/S0036023612070182

23. Zhu, X., Li, W., Guan, X. (2015). An active dealkalization of red mud with roasting and water leaching. *Journal of Hazardous Materials, 286,* 85–91. https://doi.org/10.1016/j.jhazmat.2014.12.048
24. Li, Y., Luo, X., Li, C., Millar, J., Jiang, J. et al. (2019). Variation of alkaline characteristics in bauxite residue under phosphogypsum amendment. *Journal of Central South University, 26(2),* 361–372. https://doi.org/10.1007/s11771-019-4008-8
25. Gong, Z. (2022). *Performance optimisation and mechanism of red mud denitrification catalysts (Master Thesis)*. Shandong University, Jinan, China.
26. Wu, B., Tan, Z., Ning, Y. (2021). Effects of mixing amount of red mud on strength and economic of concrete. *Journal of Henan Polytechnic University (Natural Science), 40(6),* 182–188 (In Chinese).
27. Romano, R., Bernardo, H., Maciel, M., Pileggi, R., Cincotto, M. (2018). Hydration of portland cement with red mud as mineral addition. *Journal of Thermal Analysis and Calorimetry, 131,* 2477–2490. https://doi.org/10.1007/s10973-017-6794-2
28. Liu, Q., Zhou, X., Huang, J., Luo, Z., Shao, Z. (2021). Research statue on adsorption properties and mechanism of heavy metal ions using red mud. *Chemical Industry and Engineering Progress, 40(6),* 3455–3465 (In Chinese).
29. Yuan, G., Cao, Y., Schulz, H. M., Hao, F., Gluyas, J. (2019). A review of feldspar alteration and its geological significance in sedimentary basins: From shallow aquifers to deep hydrocarbon reservoirs. *Earth-Science Reviews, 191,* 114–140. https://doi.org/10.1016/j.earscirev.2019.02.004
30. Wang, Q., Su, H., Li, C., Lyu, X. (2022). Recycling of steel slag as an alkali activator for blast furnace slag: Geopolymer preparation and its application in composite cement. *Clean Technologies and Environmental Policy, 25(5),* 1617–1629.
31. Kovtun, M., Kearsley, E., Shekhovtsova, J. (2015). Chemical acceleration of a neutral granulated blast-furnace slag activated by sodium carbonate. *Cement and Concrete Research, 72,* 1–9. https://doi.org/10.1016/j.cemconres.2015.02.014
32. Yang, K., Cho, A., Song, J., Nam, S. (2012). Hydration products and strength development of calcium hydroxide-based alkali-activated slag mortars. *Construction and Building Materials, 29,* 410–419. https://doi.org/10.1016/j.conbuildmat.2011.10.063
33. Akturk, B., Kizilkanat, A., Kabay, N. (2019). Effect of calcium hydroxide on fresh state behavior of sodium carbonate activated blast furnace slag pastes. *Construction and Building Materials, 212,* 388–399. https://doi.org/10.1016/j.conbuildmat.2019.03.328